chapter four

Scenes into Numbers: Facing the Subjective in Landform Quantification

Richard J. Pike

Contents

Keywords: *analog modeling, classification, clustering, correlation, DEM, digital elevation model, digital terrain analysis, extraterrestrial terrain, feature abstraction, feature identification, geometric signature, geomorphology, geomorphometry, hill shading, image analysis, impact craters, index numbers, landform geometry, landform interpretation, landforms, landscapes, landslide hazards, Mars, measurement, Mercury, meteorite craters, modeling, Moon, morphometry, multi-ring basins, multivariate analysis, parameterization, pattern, perception, photointerpretation, photoclinometry, photogrammetry, planetary surfaces, principal components analysis, quantitative terrain analysis, radargrammetry, redundancy, relief, river basins, sampling, sand dunes, SAR, signatures, slope, statistical analysis, surface features, synthetic-aperture radar, terrain analysis, terrain modeling, terrain perception, topography, transformation, Venus, visualization, volcanoes*

> *However tempting it may seem to leave everything to the computer, knowledge discovery is still a collaborative process that involves human expertise in a fundamental way.*
>
> Brodley, et al.[4]

4.1 Introduction

This chapter addresses the role of human factors in quantifying terrain features from remotely acquired photographs and digital images. After introducing the practice of surface quantification, this methodological essay examines six links in the chain of inference that connects the perception of topographic form with its understanding:

- defining a measurable form
- sampling a population of landforms
- choosing descriptive parameters
- measuring or enumerating parameters
- analyzing the data
- making sense of the results

Human judgment pervades not only these stages of investigation but also the analytical procedures, ten of which are discussed here.

Most examples of this uncertainty are from the author's studies of impact craters and volcanoes during early exploration of the Solar System. The chapter closes with some lessons learned from the experience.

4.2 *Surface quantification*

The traditional vocabulary by which topographic information has been extracted from a scene—"rolling hills," "strong relief," "concave slopes"—no longer suffices. Verbal, qualitative, expression of surface form not only is ambiguous but fails to deliver full content of the scene. A more quantitative approach is needed. Numerical abstraction of terrain proceeds directly from the visual appraisal of a scene. Characterization of a landscape as, say, "rolling hills" presupposes a perceptual process that links the optic array containing information about the scene[12] with a mental integration of terrain form that is not arbitrary but rather grounded in observational principles. If topography can be perceived as it is and described from criteria shared by a consensus of observers, then sufficient information must be present in the optic array to specify the terrain in concrete, quantitative terms.[20]

Measurement of the relief and pattern observed in topography is essential to understanding land-shaping processes and representing Earth's surface as the locus of human activity. Its origins—older than Renaissance hydrology, Roman civil engineering, or Egyptian surveying—are lost in antiquity. The first systematic measurement of topography preceded the early quantification of Earth's surface-form by Alexander von Humboldt and later German geographers.[34] From telescopic measurements of craters on the Moon, the astronomer Johann Schröter[60] calculated volumes of the raised rim and inner depression—and found them, on the average, equivalent (see "Schröter's Rule"[39]). Figure 4.1(a) shows Humboldt, a large crater of the type Schröter measured, and Figure 4.1(b) shows the geometric quantities that translate the visual perception of these craters into computable numbers. In describing human factors in the quantitative analysis of topography from remote data, this chapter draws heavily from Schröter's legacy.

The art, science, and technology of ground-surface quantification are known by various terms, such as (geo)morphometry.[51] Practice is mainly parametric, that is, "capturing" the character of topography by slope, relief, spacing, directional orientation, and other metrics of form.[7,48] Topography also is quantified by automated techniques of visualization, such as relief shading.[50] Recently revolutionized by the mass-production of digital elevation models (DEMs) and square-grid arrays of terrain heights,[7,51] the discipline is preparing for explosive growth as synthetic-aperture radar (SAR) and other instruments image Earth's surface and return unprecedented volumes of topographic data.[4,66,69]

Despite the common assumption that its mathematics makes it "objective," terrain quantification entails much human supervision. This subjectivity affects landforms and landscapes alike.[7] Landforms—river basins, landslides, volcanoes, sand dunes, meteorite craters—are spatially discrete and readily outlined on a map or image. Landscapes are *continuous* tracts of terrain that do not comprise a mosaic of well-defined landforms. The interpretation of

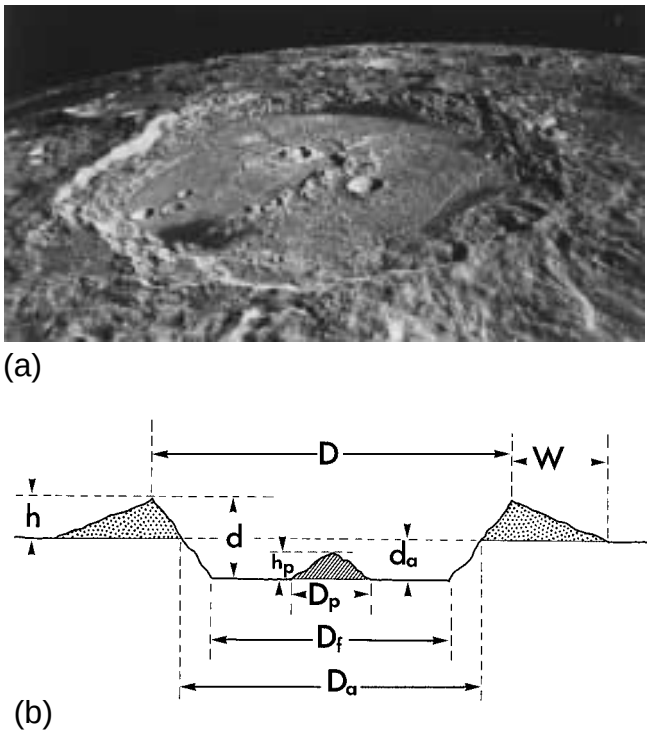

Figure 4.1 **(a)** Lunar scene at about 27° S, 81° E. The large *complex* Humboldt crater contrasts morphologically with the small *simple* craters within. Scene is 250 km across. Apollo 15 mapping-camera photo 2513. **(b)** Geometric abstraction of a lunar landform. Nine quantities that characterize the morphology of large impact craters such as Humboldt.

landforms is subjective in various respects: identifying and defining a feature, selecting and measuring its dimensions, analyzing the data, and understanding the results. Analysis of the continuous landscape introduces added uncertainties.[51] This chapter focuses on landforms, the more tractable of the two modes of surface quantification. The first step is recognition of the feature.

4.3 Landform identification

4.3.1 Landslides

The recognition of landforms remotely is sensitive to variance in human expertise.[3,8] Landslides are mapped from aerial photos in order to obtain a regional inventory of this hazard. In addition to the usual problems arising from photo quality, scale, and time of year and day, the topographic criteria for recognizing landslides are complex and subtle. Not all analysts use the same criteria or interpret them similarly.[36] Some observers are more inclusive of landslides than others; some will map both the landslide scar and the

deposit, others only the deposit; some are better at recognizing landslides in certain types of bedrock, terrain, or vegetative cover. The variance in experience and "personal equation" are evident in different inventories of landslides for the same area by different analysts. Such variations may bias statistical models of vulnerability to slope failure.[35,36] Field work can resolve some discrepancies resulting from uncertainty in photointerpretation, but on-the-ground verification is too costly for large areas. In space exploration, however, ground truth is largely unavailable.

4.3.2 Large impact craters

Remoteness of Earth's Moon and the planets poses a special challenge to recognizing surface features.[4,16] Percival Lowell's misidentification of canals on the planet Mars, a classic blunder in signal recognition, remains a caveat to all who push the limits of perception. Less celebrated examples include the long delay in correctly identifying the Moon's craters as having formed by the impact of meteoroids. The last proponents of a volcanic origin for the craters pressed their case from photographic analogies with terrestrial features,[14] a qualitative argument vanquished by the analyses of crater geometry described in this chapter.

A debate over the Solar System's largest landforms, multi-ring basins, illustrates many of the uncertainties in feature identification on the planets.[30,64] Impact craters form a size-dependent morphologic continuum[13] starting at *simple* craters, the small bowl-shaped depressions with featureless interiors shown in Figure 4.1(a). It progresses through larger, *complex*, forms with interior terraces and a flat floor surrounding a central peak or cluster of peaks—exemplified in Figure 4.1(a) by the Humboldt crater. The continuum ends in multi-ring basins, broad depressions ringed by concentric scarps. Figure 4.2 shows the archetypal lunar basin Orientale and four of its concentric raised rings. Ranging from two to perhaps six per basin, the rings vary in form and commonly diminish in relief and completeness—and thus ease of recognition—with distance outward from the center.[52,67]

Multi-ring basins were first mapped on the Moon by Hartmann and Kuiper,[17] who discovered a systematic spacing of adjacent rings: an interval of about $\sqrt{2} \times$ diameter (D), or 1.4 D.[17] Figure 4.3 reveals this spatial order in a plot of each ring diameter against that of the topographically most prominent ("main") ring in its basin. Combined, the 78 rings of 17 lunar basins define 7 linear clusters, ranked I–VII in Figure 4.3. The ranked clusters shown here all are spaced about 1.4 D apart. A similar 1.4 D interval was identified in multi-ringed craters on Mars and Mercury,[52] and Earth.[25,47] This consistency in ring spacing is important because it constrains hypotheses for the origin of the basins.[64]

Reality of the spacing interval became disputed as missions to the planets and rocky satellites returned images of older, less distinct basins.[52] The subdued and fragmented appearance of many rings, absence of the 1.4 D spacing on icy satellites, and dependence of choice of the main ring on photogeologic expertise raised doubts of even the existence of more than two

Figure 4.2 The lunar multi-ring basin Orientale. Outermost visible ring, about 930 km across, is "main" ring—equivalent to rim crest of a smaller impact crater; two faint larger rings are not evident at this scale. Lunar Orbiter IV frame 187M.

or three concentric rings per basin. Melosh[29,30] and Alexopoulos and McKinnon[1] also took issue with interpretations of basin origin that built on the constant ring spacing.[52,64] The dispute extended to Earth. Because most meteorite craters are deeply eroded, their observable features are structural—ring-shaped geologic faults and folds that formed at depth. These features are difficult to equate with their now-vanished (eroded) topographic

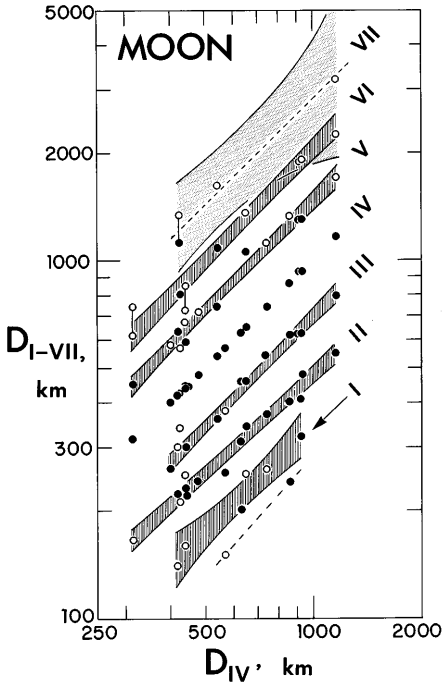

Figure 4.3 Plot exemplifying order in lunar landforms: similar spacing between 7 clusters (ranks I–VII) of ring diameters (D) for 17 basins. See text for explanation. D_{IV} is main ring. Open circles are faint rings; vertical lines join split segments of one ring. Shading shows statistical confidence for equations (at the 95% level) fit to 6 clusters; only rank VII is weak; two small rings suggest a rank below I. Orientale's 6 rings form part of second column of dots from right.

counterparts—the raised rings by which terrestrial craters are compared with planetary basins.[47] This subjectivity in linking topography to its subsurface structure weakened inferences drawn from combined Earth and planetary data.[15]

A cultural clash of authorities, recalling that of Alfred Wegener and his opponents,[38] informs the ring debate. Both disagreements arose from narrowness in expertise and the absence of a formational model. Wegener's critics could conceive of no mechanism for continental drift. Similarly, current physically based models of the impact process explain no more than two basin rings.[29,32] This prompted theoreticians—unfamiliar with the nuances of photointerpretation—to reject the more cryptic rings identified by empiricists,[30] while empiricists Pike and Spudis[52,64] rejected the theoreticians' cratering model for its failure to account for the many rings they observed. The debate ended only with recognition of 1.4 D ring spacings for basins on Venus[18,58] and for the multi-ring meteorite craters Chicxulub in Yucátán[61] and Sudbury in Ontario.[63] Rarely has agreeing on the validity of a landform and its sampling aroused such controversy.

4.4 Sampling the population

Once identified, a landform must be measured in quantities sufficient for analysis. The adequacy of a sample depends on objectives. Landslides are atypical in that the most complete inventory possible is needed for hazard mapping. A sample of about 30–50 landforms suffices for the more usual requirements, such as stable measures of correlation and other statistics. For many landforms—sand dunes, river basins, small impact craters—these modest numbers are readily achieved. This is not so for rare features—multi-ring basins, meteorite craters, some large volcanoes—for which all examples tend to be included. Lacking an adequate sample, one can either discard that landform or choose to proceed under the usual risks attending the statistics of small numbers.

A sample also should span the entire size range of the landform. Schröter's venerable "rule," for example, turned out to be wrong. Because Schröter's equipment limited his measurements to large features, he missed the small craters for which rim and bowl volumes are not equivalent.[39] Similarly, the uneven availability of images and maps limits sample size and

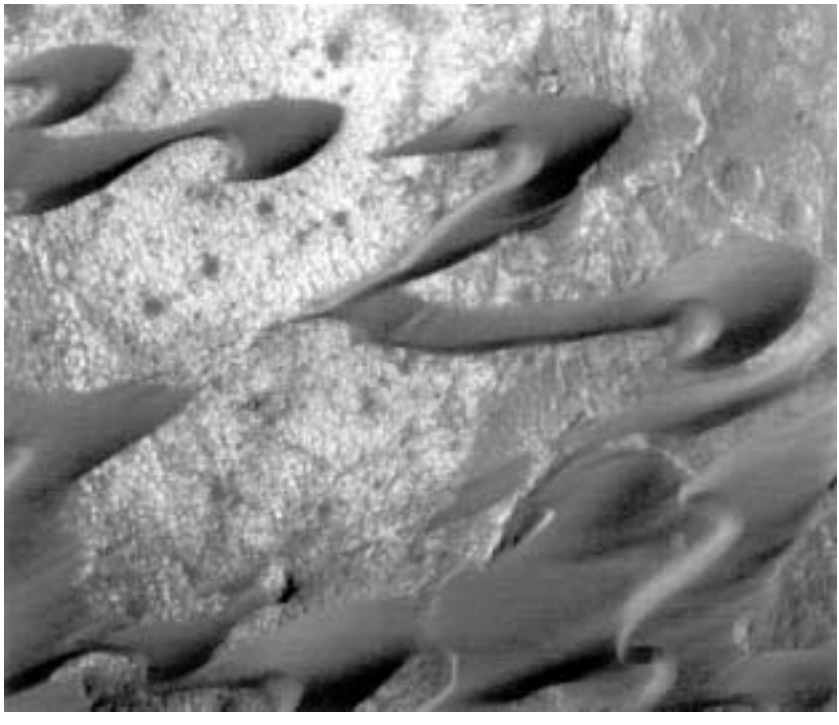

Figure 4.4 A Martian scene at 79° N, showing barchan dunes imaged at 3 m / pixel by Mars Global Surveyor in March 1999. Scene is 2.1 km across. Image P-50279.

variety.[36] Combining observations from different sources, at different scales, can result in a nonuniform data set and increase uncertainty in subsequent analysis. Finally, clarity of a landform and variations in freshness influence sampling. Well-formed features invite measurement; degraded or poorly exposed forms tend to be ignored.[36]

Figure 4.4 shows barchan dunes recently imaged on Mars, which illustrate some of the sampling issues. On Earth, these crescent-shaped landforms threaten desert settlements, the speed of their migration varying with sand supply, dune size, and terrain form.[3] Barchan dimensions, needed to model their movement and predict location, can be measured remotely,[3,57] but aerial photos and satellite images rarely span their entire size range. Recalling Schröter, instrumentation limited the sample of Sarnthein and Walger[57] to barchans more than 25 m across, leaving 200 smaller dunes unmeasured. Any size-dependent differences in the morphology of smaller barchans will go unrecorded by such incomplete ("truncated") samples, possibly leading to incorrect understanding of their mechanics of migration. Figure 4.4, by contrast, is so detailed that it can be processed to extract any parameters of barchan form—length, height, horn-to-horn width, and angles of windward and lee slopes. The linear sand dunes portrayed by shaded relief in Figure 4.5 are too small to sample any parameters accurately.

4.5 Parameters of surface form

Landforms selected for sampling must be "captured" from images and maps by describing their shape in ways that distinguish them from other landforms. This abstraction of shape is accomplished by measuring geometric attributes[22,24,60] and by recording the presence or absence of morphologic features.[45] The analyst's judgment guides both the choice of parameters and making the measurements. Selecting diagnostic parameters requires familiarity with past work, intimate knowledge of how landforms are portrayed on source maps and images, and experience in measurement. A parameter that cannot be measured accurately across the entire sample is an unwise choice, and individual landforms on which defensible measurements cannot be taken should be dropped from the sample—often a painful decision.[45]

Uncomplicated landforms, like the near-circular impact craters shown in Figure 4.1(a) and the volcano diagrammed in Figure 4.6, can be specified for most purposes by the few measures in Figures 4.1(b) and 4.6—diameters of the rim, flank, and floor; depth; and height of the rim above exterior datum.[2,41,60] The circularity index, area of an inscribed circle divided by that of a circumscribed circle, expresses symmetry of the rim-crest outline.[42,44] (Most volcanic craters, for example, have circularities of 0.40–0.70, most impact craters 0.75–0.85.) Distinction among crater sub-types requires added information—on such morphologic details as bowl shape, flat floor, terraced rim, and central peak.[45,49] The geometry of landslides, sand dunes, and most other landforms is irregular and thus harder to specify.[24]

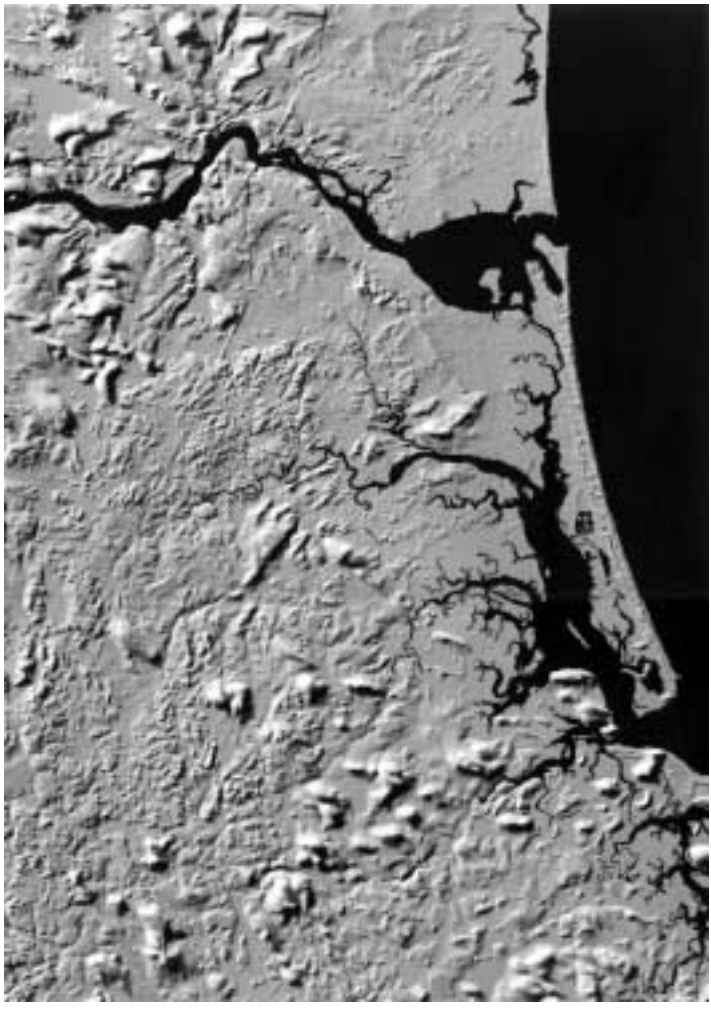

Figure 4.5 A terrestrial scene (Massachusetts). Landforms in a shaded-relief image: cluster of drumlins (lower right) and long line of small dunes (adjacent island). Computed from 30-m DEM; linears are raised roadbeds; scene is 22 km across.

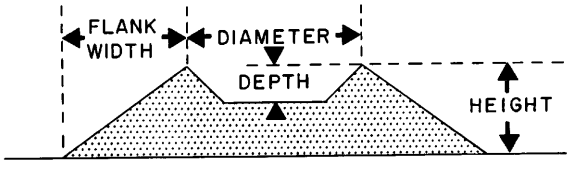

Figure 4.6 Parameters that quantify volcano shape. Profile from averaged dimensions for 12 "pseudocraters" formed by lava flowing over saturated ground. Base diameter 135 m.

Experiments with river basins have resulted in many descriptive measures, such as the hypsometric integral (elevation skewness), crenulation of the basin outline, and drainage density. Groups of river-channel segments are represented collectively, by measures that describe their topology and spatial pattern.[7,22,33,56] A good parameter, however, is of little value if it cannot be measured accurately.

4.6 Making measurements

Remote measurement of topography dates to Galileo's first estimates of relative height on the Moon from the length of cast shadows. Taken visually at the telescope, the dimensions of craters measured by Schröter and his successors varied in accuracy and precision with instrumental error, disturbances in Earth's atmosphere, location on the Moon, and the observer's idiosyncracies.[2,27] Historically, measurements of crater diameter have been consistent, but those of depth and rim height are not. Because shadow tips are indistinct, many relief estimates were low and reflect shadows that were not on the floor of a large crater, at the center of a bowl-shaped crater, or beyond the foot of the exterior rim.[44,45] Sources of vertical error did not disappear with the advent of photography.[9] Only during the post-Sputnik race to the Moon were sufficient resources committed to shadow-length photography to reduce its uncertainties to an acceptable level, by automating identification of the shadow tip.[55] Even so, the depth and rim-height data generated by the U.S. Air Force for its lunar maps were uneven in quality and required careful screening.[39,40]

Uncertainties in the remote capture of landform data remain despite advances in technology. Current methods all require human intervention. Photoclinometry ("shape from shading"), which extracts terrain slope from image brightness, is used on Mars and satellites of the outer planets where photogrammetry cannot be applied.[65] It requires careful internal calibration.[21] Photoclinometry's inverse, digital relief-shading, creates a brightness map from terrain slope. It, too, relies on experience to generate a high quality image.[50] The drumlins (low, rounded hills formed beneath glaciers[26]) shown in shaded-relief in Figure 4.5 are sufficiently clear that their length, width, and correspondence to an ellipse can be measured. Although photogrammetry yields the most accurate relief values, pre-Apollo maps contoured photogrammetrically[37] decreased in reliability with distance from the center of the lunar disk and had to be used selectively.[39,40] Experts still must judge the suitability of base / height ratios for planetary photogrammetry, as well as evaluate the performance of SAR imaging degraded by steep or forested terrain.[11,54]

The inaccuracies inherent in images, maps, and DEMs obtained by remote sensing are compounded by ambiguities in measuring the landforms on them. Even morphologically uncomplicated features, such as the radially symmetric craters in Figures 4.1(a) and 4.2, can require many operational

decisions.[44,45] Photogrammetry from returned Apollo film improved the precision of lunar data but did not eliminate the need for human judgment. For measuring crater-rim height in uneven terrain, for example, one must choose several elevations on the rim crest, decide on a reasonable radial distance outward, and then choose more heights.[44] That radial distance, rim width, remains the most uncertain of all crater dimensions, an ambiguity not eliminated by laser altimetry[10] or planetary DEMs.[23] Crater diameters can be uncertain. Isolated fragments of subdued basin rings must be carefully mapped before fitting a circle to them.[52]

Similar ambiguities complicate the quantification of terrestrial landforms. Measuring the base diameter of a volcano that merges gradually into the surrounding terrain can require a geologic map to locate the extent of the form. Obtaining the rim outline of a volcano's summit crater to measure its circularity also can be difficult because many rims are fragmentary or eroded; reconstructing a rim crest requires good judgment and restraint. Analogous problems in defining landform extent from remote data arise in measuring landslides, glacial cirques (erosion hollows in mountainous terrain[8]), and the drumlins shown in Figure 4.5. The many small decisions required in measuring these landforms are an essential prelude to their analysis.

4.7 Landform analysis

Landforms are interpreted from their measurements by methods that are subjective, despite the scientific objectivity sometimes claimed for them. Ten analytical practices are discussed in this section:

1. Arraying landforms by size or morphology
2. Stratifying a sample by relative age
3. Searching for correlations
4. Assigning varying importance to descriptive data
5. Transforming a parameter's scale of measurement
6. Deriving index numbers
7. Sorting variables to reduce redundancy
8. Obtaining an optimal set of parameters
9. Classifying landforms by multiple measures
10. Modeling morphometric relations and formational process

4.7.1 Initial sorting

Subdividing a landform sample prior to numerical analysis is something of an art. Interpretation of impact craters, for example, requires recognizing qualitative differences within the size-dependent array of morphologies. Dence[5] distinguished the first of these transitions, from a simple (deep, bowl-shaped) to a complex (shallow, several interior features) shape, in Earth's meteorite craters. Figures 4.7 and 4.8 illustrate (in detail not present in

(a)

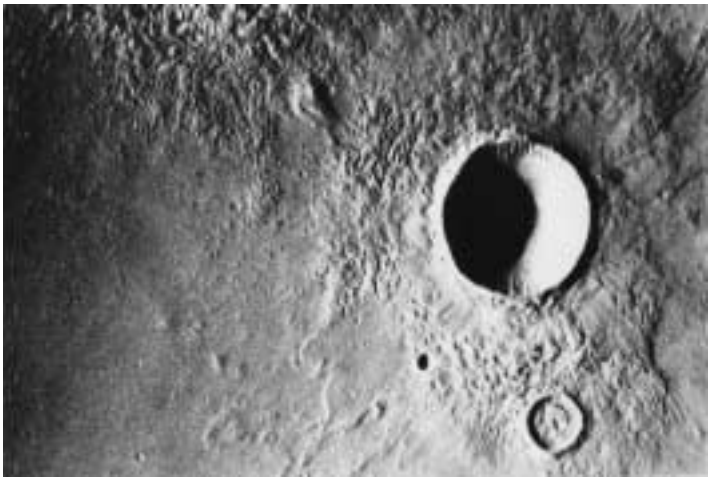

(b)

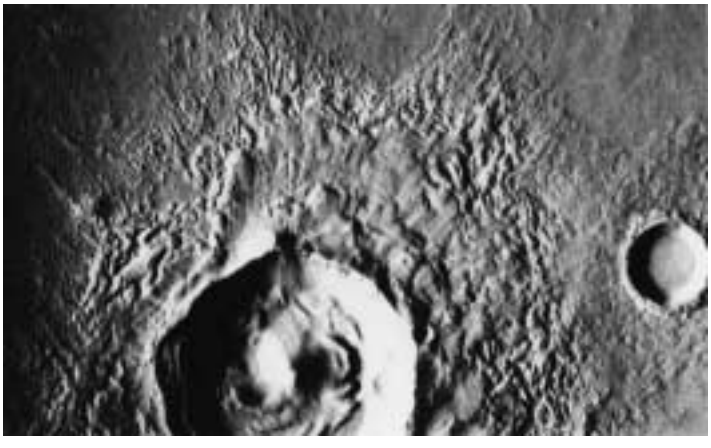

Figure 4.7 A quantifiable contrast in landform morphology: examples of fresh simple (**a**) and complex (**b**) impact craters on Mars. See text for explanation. Craters are 8 and 14 km across. Viking Orbiter frames 645A09 and 645A01.

Figures 4.1(a) and 4.2), this transition for craters on Mars. The simple crater in Figure 4.7(a) differs qualitatively from the larger complex crater in Figure 4.7(b)—with its central peak, flat floor covered with slumped material, and scalloped and terraced rim. The data for seven of these morphologic features in Figure 4.8 demonstrate the power of presence/absence identifications, judgment-laden as they are, in quantifying this distinction. The transition is defined by averaging diameters of craters containing the largest simple features and smallest complex features. This diameter, about 5 km on Mars,

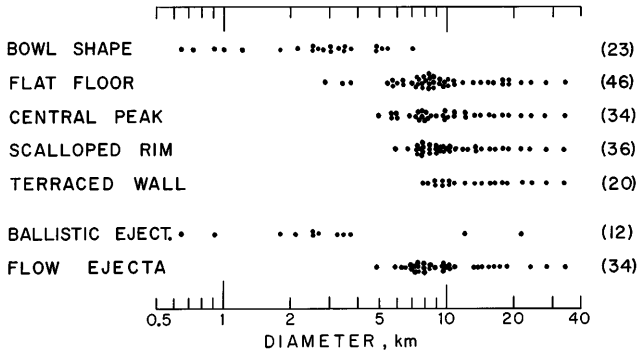

Figure 4.8 Qualitative criteria that quantify the morphologic transition from simple (bowl shape, ballistic ejecta) to complex (other five features) craters. Presence/absence of features for 73 craters (205 dots) on Mars, from Viking Orbiter images.

differs from planet to planet according to gravity and rock materials and is critical to understanding controls on the impact process.[49,59]

Neglecting qualitative differences can lead to overgeneralization. The first quantitative relation to link craters on the Earth and its Moon, a continuous depth/diameter curve, did not separate simple from complex morphologies.[2] Making that distinction, however, revealed that the relation actually consists of two distinct, linear, segments—inflected at the transition.[39] This "dog-leg" break can be seen on page 99, in Figure 4.10(a). Similarly, concentric rings in impact basins on Venus are spaced at the 1.4 D interval described earlier.[58] They do not vary from this value as claimed by Alexopoulos and McKinnon,[1] who had combined three disparate types of craters and basins rather than plotting their data separately.[18]

Other types of landforms must be sorted. The author subdivided over 650 volcanoes by eruptive process and rock type before deriving metric profiles to compare their shapes with those on planetary images.[43] Profiles for the 20 classes in Figure 4.9 were computed from averages of the four dimensions in Figure 4.6 plus the circularity index. Assignment of a volcano to a class was based on the author's evaluation of descriptions in the literature. There is no "correct" number of these classes, which grew from the initial four[41] as volcanoes were added to the sample and larger classes were judged excessively mixed in geometry and geology. Success in subdividing large classes was confirmed by reduced variance in descriptive statistics for the five parameters. Because erosion rates on Earth differ widely in their effects, these volcanoes could not be stratified further by age or degree of degradation.

4.7.2 Stratifying the sample

Subdividing impact craters by age on the Moon where erosional changes in landform are more predictable was not only possible, but led to inferences of surface-shaping processes. Baldwin's[2] depth/diameter graph for the first

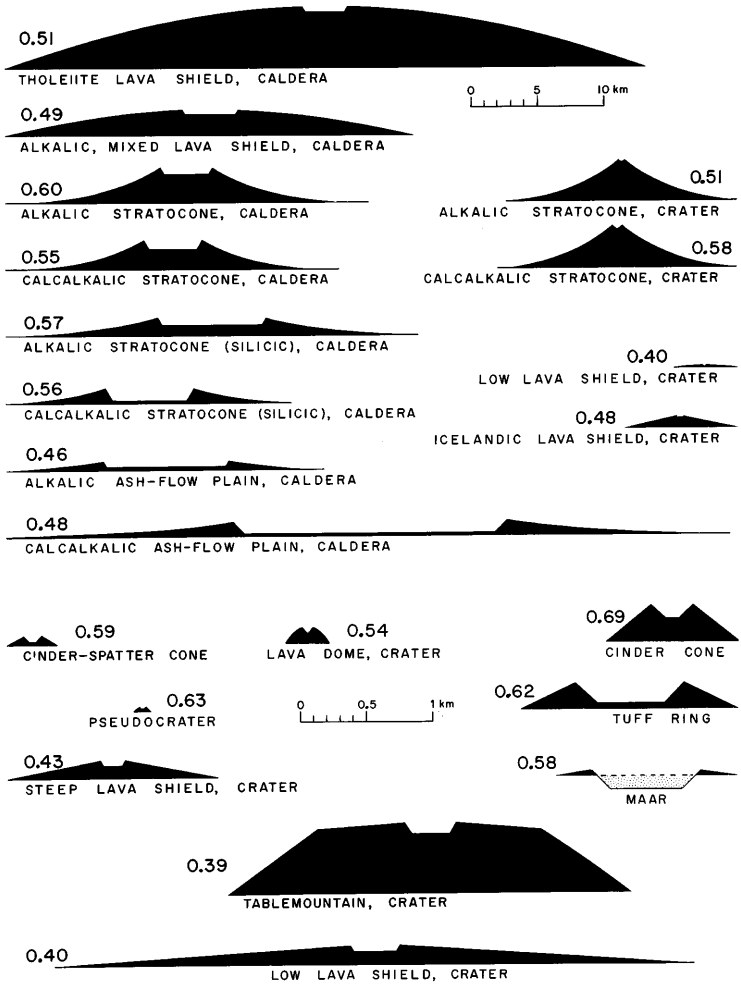

Figure 4.9 Geometric models for 20 volcano classes from measurements on maps and images. See text for explanation. Numbers give circularity of crater rim. Vertical exaggeration 2×; scale of lower nine profiles 10× that of upper 12 (low shields shown at both scales).

time linked lunar craters with terrestrial meteorite craters and craters formed by experimental explosions. Contributing to Baldwin's success was his inclusion of only the freshest-appearing landforms. Although subjective, his five age groups reflected the judgment of a keen observer. This deliberate winnowing excluded old, eroded craters that would have violated the cardinal rule of fitting an equation only to like phenomena.

Stratification by crater age also was instrumental in deciphering the geology of the Moon. Pohn and Offield devised an ordinal ranking of large

craters from their visual appearance on Lunar Orbiter IV images.[53] By noting presence/absence or degree of preservation of rim-wall terraces and other secondary features, they assigned craters to one of nine decreasingly pristine classes and equated that state of degradation with relative age. This system, implemented by geologists expert in lunar mapping, created a workable sequence of rock formations and geologic events for the Moon.[67] A model of crater age based solely on geometric criteria, by a less experienced observer,[40] was not as successful because it reflected fewer agents of crater modification. Total neglect of relative age has lead to negative results, such as the failure of Green's[14] correlation analysis to distinguish the Moon's craters from terrestrial *calderas* (large volcanic craters).

4.7.3 Correlation

Correlating the right parameters within a properly stratified sample of landforms can lead to strong inference. Baldwin's[2] depth/diameter curve correctly linked craters that formed by explosive release of energy, but did not exclude the volcanic hypothesis. The plot of 1100 landforms in Figure 4.10(a) reveals why. Four of the 20 types of volcanoes shown in Figure 4.9—terrestrial calderas, cinder cones, and maars and tuff rings (small explosion craters), plus lava domes on the Moon—occupy the same graphical field in Figure 4.10(a) as impact craters and their genetic analogs—lunar craters, experimental explosion craters, and meteorite craters.[41] The two processes clearly overlap. Not until the author established correlations for rim height, width, and circularity[41,42] were volcanoes[14] eliminated as geometric analogs. The plot of 425 landforms in Figure 4.10(b) shows that crater height/depth, unlike depth/diameter, does discriminate landforms by process. Volcanoes occupy a different field than impact craters and their analogs.[41] The maars and tuff rings (see Figure 4.9) that plot with impact craters form (explosively) only in the presence of abundant ground water[62]—virtually absent on the Moon—and thus are excluded as lunar analogs. Reaching this conclusion from Figure 4.10(b), however, required specialized knowledge beyond the plotted data.

Landform correlations established from remote data tend to be revised as sensing technology improves with each mission. New, higher-resolution information may add nothing new, or it can force reexamination of earlier conclusions.[2,39] The author's revision of the simple-to-complex transition for craters on Mercury, for example, was so substantial that it led to the establishment of a basic correlation between crater morphology and surface gravity for the rocky planets.[49] Eventually, however, diminishing returns set in. Data will attain sufficient accuracy that no further revision of measures is justified from incrementally better information. Recognizing when this has occurred is one of the finer judgment calls in the remote study of landforms. Another fine point is the uneven quality of descriptive data.

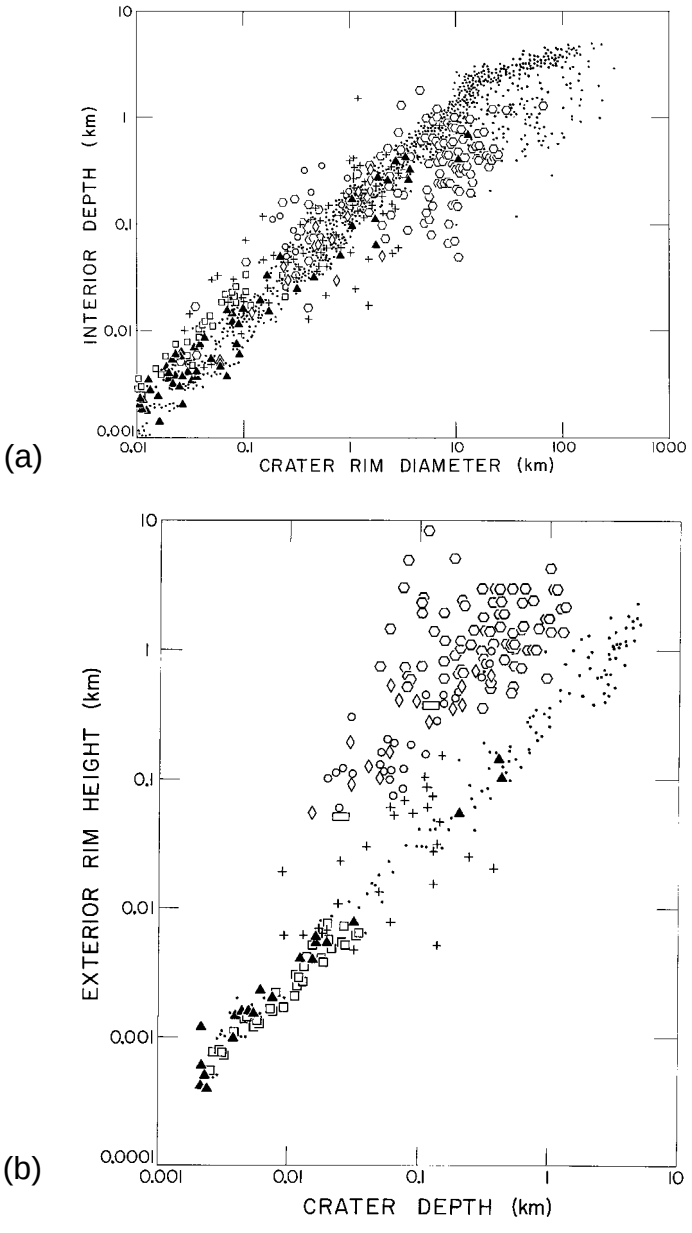

Figure 4.10 Good and bad discriminants of landform process. **(a)** Depth diameter fails to separate craters formed by different agents. Terrestrial calderas (hexagons), cinder cones (circles), maars and tuff rings (crosses), explosion craters (squares), meteorite craters (triangles), lunar craters (dots), and lava domes (diamonds). **(b)** Height / depth successfully divides volcanoes (upper cluster) from impact craters (lower cluster). Two rectangles are volcanic domes on Earth.

4.7.4 *Weighting*

Some landform measurements and parameters are superior to others, but whether to weight the data accordingly is seldom addressed. Weighting, when it is attempted, always hinges on human judgment. In systematizing the analysis of basin rings on the Earth, Moon, Mars, and Mercury through correlation, Pike[47] and Pike and Spudis[52] addressed the uneven quality of their 300 rings by assigning a weight to each diameter: 3 for unambiguous rings, 2 for less satisfactory identifications, and 1 for the least certain interpretations (the open circles in Figure 4.3). These values, although arbitrary, reduced the greater arbitrariness that would have prevailed by including cryptic with obvious rings in the same calculation. Another example of weighting is given later in this chapter, in discussing principal components analysis. Weighting the data, however, is the only way to improve a correlation.

4.7.5 *Transformation*

The scale of measurement chosen for a landform metric influences correlation. Further contributing to the success of Baldwin's[2] depth/diameter plot was his use of logarithmic scales. Prior analyses[28] had not corrected for the severe skew in the frequency distributions of crater dimensions, very few of which follow the normal bell-shaped curve. The importance of this difference cannot be overestimated; all successful crater morphometry since Baldwin's has employed logarithmic scaling.[45,59,68] Ratios of parameters, such as those in Table 4.1, may require different transformations. Landform descriptors are not transformed without risk of distorting the data, and the distribution of each measure must be evaluated. The extra care, however, will be repaid by improved correlations (as in Table 4.1), narrower margins of error, recognition of sub-categories of features, and more robust index numbers.[42,43]

Table 4.1 Correlation coefficients (**r**) for pairs of transformed parameters that describe 402 lunar and terrestrial impact craters and volcanoes*

Variables	1	2	3	4	5	6	7
1. Circularity	1.00						
2. Height/depth	−0.47	1.00					
3. Width/diameter	−0.44	0.73	1.00				
4. Height/diameter	−0.38	0.77	0.84	1.00			
5. Depth/diameter	0.07	−0.19	0.29	0.48	1.00		
6. Height/width	−0.01	0.29	−0.01	0.52	0.41	1.00	
7. Depth/width	0.46	0.79	−0.68	−0.40	0.46	0.31	1.00

*Absolute values of $\boldsymbol{r} < 0.25$ not significant at 0.01 confidence level. Parameters were transformed, respectively, to x^3, $\log x^{-3}$, $\log x^{-2}$, $\log x^{-3}$, $\log x$, $\log x$, and x^{-3}. Parameters defined in Figures 4.1(b) and 4.6 and in the text.

4.7.6 *Index numbers*

The ratios in Table 4.1 exemplify combinations of measures that carry greater descriptive power than individual measures. Derivation of these index numbers from remotely sensed data is a heuristic process entailing familiarity with the landforms and a flair for experimentation. Figure 4.10(b), which shows that the ratio of landform height to depth separates most volcanoes from most impact craters, originated in trial plots of a few parameters that might prove more diagnostic than depth/diameter. From this tentative start the author recognized that the main difference between volcanoes and impact craters could be quantified: a broad form with a small summit crater located well above the surrounding landscape vs. a low and narrow rim surrounding a large depression excavated in the precrater terrain. This contrast is revisited below in combining all seven index numbers in Table 4.1,[42,44] where tests for parameter redundancy played an important role.

4.7.7 *Data sifting and redundancy*

Decisions to retain or discard landform descriptors are subjective and not always determined by statistical testing. One guideline is redundancy. Two or more parameters can express much the same basic attribute of form; if very similar, one of them may be extraneous. Including similar parameters in an analysis can reduce its descriptive or discriminating power by giving undue weight to one attribute. Two such metrics, the hypsometric integral [(mean elevation − minimum elevation)/(maximum − minimum elevation)] and skewness of elevation, characterize continuous terrain as well as discrete landforms.[7] Figure 4.11 shows that these quantities, computed from 1:24,000-scale maps, describe the same attribute of form for 14 small river basins in the U.S. According to the statistics for this correlation, 95% of the variance in one parameter is accounted for by the other—probably sufficient to drop one measure with little loss of information.

Redundancy is an ambiguous property, in that some correlated measures differ enough in their descriptive capability to warrant retaining both. Local relief (highest minus lowest elevation within a defined area) and slope angle are two vertical constituents of terrain roughness (spacing is its horizontal constituent). Because slope traditionally is measured over short distances, whereas relief is computed over a large area, one metric characterizes fine-scale roughness and the other coarse-scale roughness—a distinction worth preserving. Thus, it is not always desirable to pare down a data set to strictly uncorrelated descriptors. Where an exhaustive description of form is required, it may be wise to include as many metrics as practicable. Much of the art in screening variables for landform characterization lies in knowing which course to follow.

Expertise in exploratory data analysis, an intuitive process, is helpful in sorting descriptors. There are many ways, for example, to compare

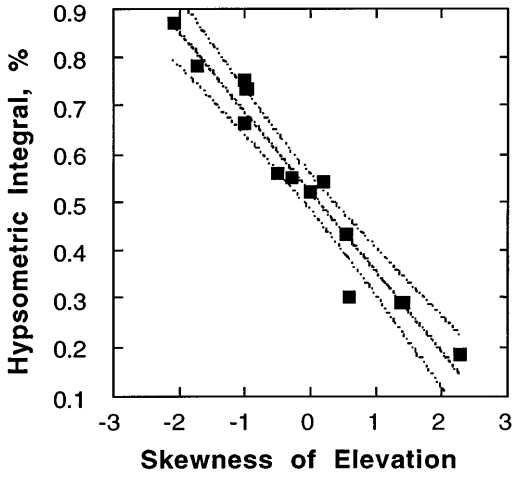

Figure 4.11 Redundancy in landform description. Inverse correlation of two similar parameters, skewness of elevation and hypsometric integral, for 14 river basins (see text).

parameters by arranging the correlation coefficient **r** in tables or diagrams.[7,33] In Table 4.1, correlations among seven index numbers computed for impact craters and volcanoes show that only variables 2, 3, 4, and 7 are closely related—albeit not to the point of redundancy. Large tables of this type[18] defy such a ready grasp of the interrelations, but a large number of variables can be sorted visually by color-coding the **r** magnitude (>0.90, 0.80–0.89, 0.70–0.79, etc.), arraying the coded **r**s for each variable in columns from highest to lowest, labeling the **r**-value that indicates statistical significance of the correlation, and finally rearranging the columns in order of diminishing number and strength of the correlations.

While nominally more "objective" than visual inspection in evaluating redundancy, multivariate techniques also require informed judgment. Principal components analysis (PCA), illustrated in Table 4.2, has reduced the matrix of **r** values for the seven measures in Table 4.1 to just four independent components—which express, in descending order of explanatory capability, the four fundamental attributes contained in the data.[42,44] The relative order of the PCs, while reasonable, should be accepted cautiously, for it depends as much on the number of contributing variables as on their intrinsic variance. In Table 4.2 the five high-scoring variables 1–4 and 7 dominate PC–1 (49%), depth / diameter and depth / width (measures of terrain slope) comprise much of PC–2, while rim-crest circularity is the only important constituent of the weak PC–4. Not all PCs are easily understood in terms of constituent variables; PC–3 has no clear-cut interpretation. One of the objectives of reducing redundancy by these procedures is to converge on a signature.

Table 4.2 Principal components (PC) analysis of seven parameters, based on correlation coefficients in Table 4.1, for 402 craters and volcanoes*

Variables	PC-1	PC-2	PC-3	PC-4	Variance
1. Circularity	−0.61	0.19	−0.01	0.77	1.000
2. Height / depth	0.93	−0.12	0.31	0.16	0.995
3. Width / diameter	0.91	0.05	−0.39	0.13	0.996
4. Height / diameter	0.88	0.46	−0.02	0.10	0.996
5. Depth / diameter	0.09	0.87	−0.47	−0.07	0.995
6. Height / width	0.21	0.76	0.61	−0.02	0.997
7. Depth / width	−0.76	0.61	0.02	−0.16	0.978
Variance	3.46	1.98	0.85	0.67	6.959
% total variance	49.4	28.3	12.1	9.6	99.4

*Values are PC scores of each parameter on first four components. PCs 1–4 yield nearly complete solution (99.4%). PCs 5–7 (not shown) add < 1% of total variance.

4.7.8 The geometric signature

Enzmann's concept of a signature, "a set of measurements sufficient to identify unambiguously an object or a set of objects,"[6] has adapted well from remote sensing to landform analysis. The geometric signature is a suite of measures sufficient to distinguish a landform or its formational process(es) from all others.[48] No specifications exist for a signature, which is arrived at by intuition and experiment. It invokes four postulates:

1. The perception of landforms in a scene can be abstracted by discrete measures
2. The measures must represent the attributes that give a landform its unique character
3. This character is inherently multivariate; no one "magic number" suffices to "fingerprint" a feature or interpret its origin
4. Characterizing landforms is a statistical problem

Signatures such as the set of seven parameters in Tables 4.1 and 4.2 provide the operational tool for classification.

4.7.9 Classification

Grouping or separating remotely sampled features by a signature can furnish clues to landform process, but classification procedures rely on the analyst's expertise at every step. The first of two experiments described here retested, from more extensive data, the hypothesis that origin of the Moon's craters could be inferred from their geometry alone. To do this, the author compared 400 landforms—from 23 classes of lunar craters, meteorite craters, and terrestrial volcanoes—across the seven ratios in Tables 4.1 and 4.2 by cluster analysis.[42,44] This two-step procedure is *unsupervised:* "training samples" are not used to specify a desired outcome.

Principal components analysis first reduced the seven parameters, properly transformed (see Table 4.1), to four PCs that provide a less redundant signature (see Table 4.2). A clustering algorithm then sorted the scores (correlations of each landform with each PC), weighted by the percent variance explained by each PC. These scores determined a measure of similarity, the distance function by which an algorithm sorted the landforms into a hierarchical array. Although interpreting these arrays can be subjective, the resulting classification shown in Figure 4.12 is unambiguous. This

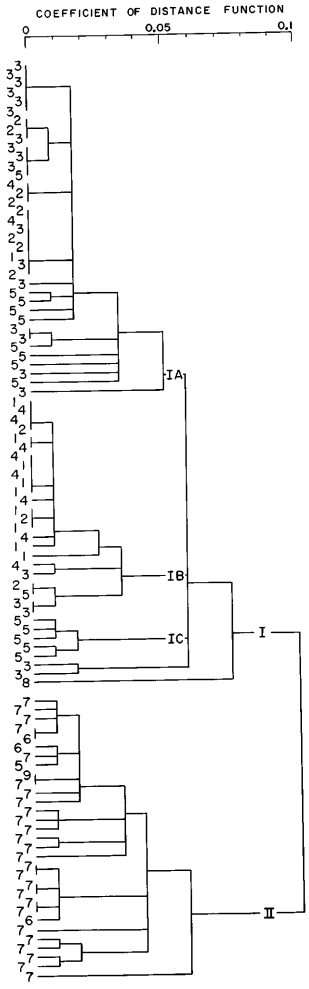

Figure 4.12 Inference of process from landform shape, I. A seven-parameter classification groups lunar craters with Earth's impact craters (I) not volcanoes (II). See text for explanation; 402 craters (numbers 1–9, every fourth shown). Classes 1–5 and 8 are lunar, meteorite, and explosion craters; classes 6, 7, 9 are volcanoes. Distance function is low for similar craters; horizontal lines show value at which each crater joins group.

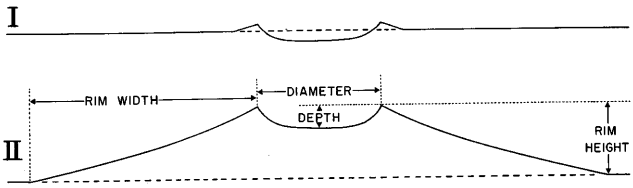

Figure 4.13 Geometric models contrasting "excavational" (I) with "constructional" (II) landforms, from classification in Figure 4.12. See text for explanation. Scaled to same rim diameter; respective mean values of crater circularity are 0.78 and 0.64; vertical exaggeration 2×.

dichotomous outcome reveals how dramatically lunar craters resemble Earth's meteorite craters, but differ from all of its volcanoes save the maars and tuff rings explained earlier. Cluster I (classes 1–5, 8) consists of lunar, meteorite, experimental, and explosion craters; cluster II (classes 6, 7, 9) includes volcanoes on Earth, the Moon, and Mars.

Contrasting profiles in Figure 4.13—computed from averaged values of height, depth, diameter, and width (see Figure 4.6)—summarize the results in Figure 4.12. The "excavational" (impact) processes that created the landforms in cluster I (275 samples) have been correctly distinguished from the "constructional" processes that built the volcanoes in cluster II (125 samples).[42,44] The higher circularity for cluster I reflects the radial symmetry imparted by the point-source release of impact energy. Judgment and intuition were essential to the success of this experiment. Classifications based on untransformed ratios or raw dimensions rather than ratios, for example, were inconclusive. Weighting the clustering required evaluation of the components. PC-1, with half the total variance, expresses the key discriminant: proportion of crater volume to that of the raised rim or volcanic construct. This attribute, evident in individual variables 1–4 in Tables 4.1 and 4.2, is so diagnostic that unweighted PCs would have invalidated the analysis.

A second experiment in multivariate classification compared over 700 volcanoes to infer the eruptive style of planetary volcanoes from the morphometry of terrestrial features. The seven-parameter signature that clearly distinguished impact from volcanism in Figures 4.12 and 4.13 did not discriminate well among eruptive styles. Nor did it display the full range of morphologic variation that the author knew existed in the 31 classes of volcanoes (increased from the 20 shown in Figure 4.9). Plotting PC scores for components on two- and three-axis diagrams (not shown) grouped most volcano classes fairly well, but the author's familiarity with volcanoes suggested that a key attribute was still missing.

Further experimentation revealed the missing descriptor to be volume of the landform. Average volume was computed for each class from the topographic profile of one fresh, well-formed volcano. The author's choices of examples so clarified morphometric relations that the simple plot of volume against rim-crest circularity shown in Figure 4.14 sufficed to array the

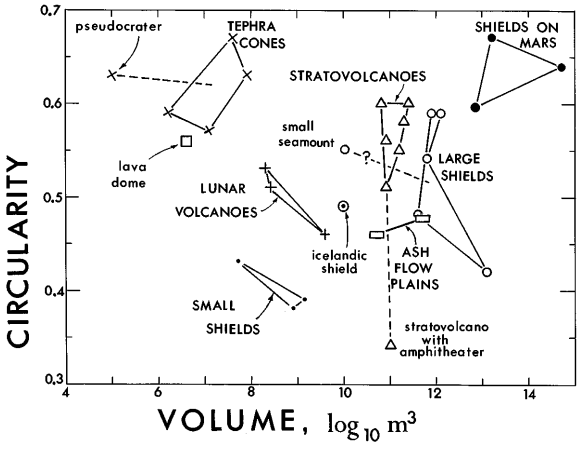

Figure 4.14 Inference of process from landform shape, II. Two parameters classify 31 volcano types into many fewer "process groups." Two of these groups resemble lunar and Martian volcanoes (see text). Symbols and solid lines group related styles of eruption; dashed lines show affinity of classes that form under unusual conditions.

31 classes in just a few groups, which correspond to the major eruptive processes and products. Four large groups—tephra (ash) cones, small lava shields, large constructs of ash and lava (stratovolcanoes), and large lava shields—account for 18 of the 25 terrestrial classes. (Discussion of the remaining seven classes lies beyond the scope of this chapter.) Adjusting volumes for differences in planetary surface gravity, moreover, moved the three Martian and three lunar classes to the left to exactly align, respectively, with large and small terrestrial shields. This alignment (not shown in Figure 4.14) suggests that volcanoes on Mars and the Moon do not form in exotic ways, but rather develop by two of the mechanisms that create Earth's chief types of volcanoes: the building of large and small lava shields. The interrelations among landforms described by the classifications in this section constitute an important type of model.

4.7.10 Modeling

Models are numerical or conceptual abstractions that aid in understanding natural phenomena. "Model" is an elastic concept, embracing interpretation and explanation as well as description and experimental analog. Human decision making colors all attempts to model landforms from remotely sensed information. Geometric models, which structure relations among descriptive measures, are the least subjective.[24,33,52] They include the 3-D abstraction of craters in Figure 4.1(b), the statistical order of basin-ring spacing in Figure 4.3, and the morphologic transition defined in Figure 4.8.

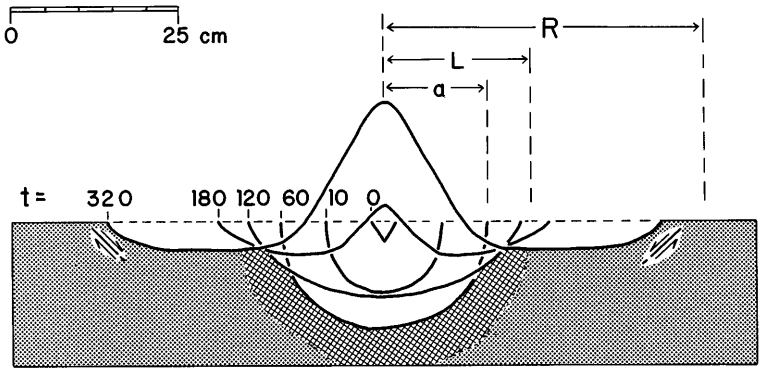

Figure 4.15 Analog model of a cratering process. Filmed experiment of impact into water shows growth of excavation cavity. See text for explanation of distances **a**, **L**, and **R**. Profiles at same scale and location in target chamber, at times **t** in msec after impact. Ejected material and raised rim omitted for clarity.

Landform classifications, such as the bivariate plot of volcanoes in Figure 4.14 and the multivariate parsing of craters in Figure 4.12, are taxonomic models.

Laboratory experiments are attempts to scale the formation of surface features, but such analog models do not necessarily simulate physical processes. They only imply. Figure 4.15 shows a model of impact cratering that scaled the strength of the target rocks as a fluid. Successive stages in the growth of a liquid-impact crater mimic the sequence thought to excavate a sombrero-shaped transient (temporary) cavity during formation of a meteorite crater.[46] The crater in water reaches its greatest depth at **t** = 60 msec (radius **a**) and then grows laterally at **t** = 120 to uplift the central peak and disrupt an inner region at radius **L**. Inertial recoil of the crater center drives late-stage growth. Uplift of the crater floor *before* gravitational collapse of the rim is consistent with the observation of central peaks and flat floors before (i.e., in smaller craters than) rim-wall terraces in the simple-to-complex transition on Mars (see Figure 4.8) and elsewhere.[49] Radius **R** at **t** > 320 marks the location of the final rim crest (not shown), which collapses in analogy to the terracing and faulting in meteorite craters (arrows).

Physically based calculations have mathematically simulated impact cratering and other surface-forming agents.[22,29,62] While more sophisticated than geometric models and more quantitative than analogs, such process models build on complex assumptions of their own and are no less the product of human decision making.[23,32] None of the several models proposed for the origin of concentric basin rings, for example, has achieved widespread acceptance.[31,52] Either they explain only rings within or outside of the main crater rim (rank IV in Figure 4.3), or require too many leaps of faith or logic, or are insufficiently quantitative.

Landform models derived from remote data can address more applied objectives. Newman et al.[35] and Nilsen et al.[36] translated the spatial distribution of discrete landslide deposits into a continuous statistical surface showing relative vulnerability to slope failure over a large area. Their semi-quantitative model, which ranks landslide vulnerability for part of northern coastal California, required a number of judgment calls in combining three constituent maps—geology, angle of ground slope, and a landslide inventory compiled by aerial photo interpretation. Ordinal (I-VI) categories of landslide vulnerability were assigned to six intervals of slope within each geologic unit, based on informed judgments of landslide prevalence within each slope interval. The map resulting from this model, while not wholly "objective," is consistent in its estimation of the hazard. Whatever the origin or purpose of the various types of models, however, most of them lead to a better understanding of surface-shaping agents.

4.8 Interpretation

Of the issues considered in this chapter, it is the inference of landform process that leaves the widest latitude for human judgment. Impact cratering illustrates this uncertainty. For such distant features as the rings of planetary impact basins, experts have yet to forge a strong link between form and process. The existence of multiple rings is admitted by former skeptics,[31] for example, but until the physics responsible for the 1.4 D spacing is understood, it cannot be known whether the rings formed—or perhaps were only located—by a wave mechanism,[52] a tectonic process,[32] or a scenario not yet proposed. On the other hand, the impact origin of smaller craters is no longer at issue,[2,42,45,62,67] and interpretations of the process now focus on details.[10]

Figure 4.16 is a general interpretation for complex impact craters based on the model in Figure 4.15 and other observations. Figure 4.16 is scaled to the averaged dimensions of Martian craters; its geologic detail summarizes field data from four well-studied meteorite craters.[45] The transient cavity of excavation (compare Figure 4.15) comprises the broad shallow zone above layer

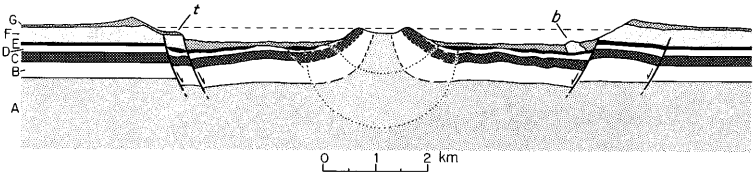

Figure 4.16 Interpretation of complex impact craters. Profile from measurements of Martian craters; geologic cross-section from terrestrial field data. Upper dotted arc is inner excavation cavity. See text for explanation and significance of rock strata A–G; arrows show faults.

E plus the deep central zone (small dotted arc). The large dotted arc marks the deep inner zone of total fragmentation and perhaps fluidization of the target rocks[29] (compare Figure 4.15). Uplift of the crater center has exposed and steepened rock strata **A**–**C** and distorted strata **D** and **E**; layer **F** has been stripped out of crater and forms slump block **b** and terrace **t** (by faulting: arrows); layer **G** is ejected material or fractured rock within the crater. Although Figure 4.16 explains many features of complex craters, it is not the sole interpretation.[29] Whether uplift of the crater floor or collapse of the rim is the dominant mechanism driving the transition from the simple to the complex morphologies shown in Figures 4.7, 4.8, 4.15, and 4.16 continues to be debated.[18,31,49] These uncertainties remain despite the field evidence from Earth's meteorite craters and the cumulative experience of many experts.

4.9 Conclusions

Human subjectivity in the task addressed by this chapter—imposing geometric order on landforms from remotely sensed information—can be reduced by developing expertise to make better operational decisions. Guidelines to more informed decision making include the following:

1. Define rules for identifying and measuring surface features
2. Reduce landforms to basic elements of shape (facets and lines)
3. Choose measurable elements common to many forms
4. Devise quantitative descriptions for qualitative features
5. Avoid incomplete samples
6. Expect landforms to vary in shape with size and age
7. Anticipate non-normal distributions of descriptive measures
8. Plot data to screen them visually before making calculations
9. Avoid inapt "apples / oranges" correlations
10. Explore the information: examine old data in new ways and new data in old ways
11. Avoid losing insights into data through their uncritical manipulation by computer

Sound judgments in landform quantification clearly relate to expertise in image interpretation, but who qualifies as an expert? One theme of this chapter has been disagreement among authorities, whose expectations commonly reflect the ruling paradigms of their respective fields. Disputes start at a low level: experts may not agree on what constitutes a valid observation, let alone "evidence." At a higher level, experts may reject results reached by analytical practices that differ from those of their own discipline; for example, theoretical vs. empirical modeling. These problems are embedded in the sociology and psychology of science and not easily resolved. Developing the expertise is more readily achieved, for landform quantification is a skill that can be learned.

In outlining a formal course of instruction, the author identified ten general topics:

1. *Conceptual framework*—philosophy of landform quantification, theory, perception and cognition
2. *Enabling technology*—image-processing, geographic information systems (GIS), knowledge-based feature recognition
3. *Elevation sampling*—map contours, profiles, DEMs
4. *Data structures*—spatial arrangements of points, lines, and areas for height derivatives
5. *Z measures*—relief, slope, profile curvature, hypsometry, other height derivatives
6. *X, Y measures*—location, extent, direction, arrangement, texture
7. *X, Y, Z measures*—3-D attributes, scale variance, self-organization (fractals)
8. *Analysis*—sampled in this chapter
9. *Synthesis*—landform taxonomy, parsing a scene, combining with nontopographic data, etc.
10. *Dynamic morphometry*—simulation and interpretation of processes to model landscape evolution[51]

Excepting theory, all these areas are fields of active research.[51] While it is capable of prediction, landform quantification is largely empirical and lacks unifying principles. Enough empirical relations may now have accumulated on which to base a general theory, but the direction remains unclear. An obvious path to theory lies through geomorphology, the established science of landforms. Alternatively, a scale- and process-independent theory based on mathematical geography might be more flexible. It would rely less on physical processes and laws than on spatial properties of relief and topologic relations derived from graph theory.[51] But, would a stronger theoretical foundation reduce the operational subjectivity described in this chapter?

Despite the uncertainties introduced by human factors, surface quantification from remotely sensed information has progressed steadily in the 200 years since Johann Schröter measured craters on the Moon. This chapter has described only a few of the discipline's recent achievements. Driven by current needs to accelerate the processing of remote imagery,[4,19,20] landform quantification is poised to make its most valuable contributions yet from the terrain data generated under such programs as the 2000 Shuttle Radar Topography Mission. Among these prospects are improved defense capabilities, more accurate appraisal of water resources, real-time warning of natural hazards, a deeper understanding of changes in the Earth's surface through time, and more refined criteria for guiding urban development and locating transportation facilities.

References

1. Alexopoulos, J. S. and McKinnon, W. B., Large impact craters and basins on Venus, with implications for ring mechanics on the terrestrial planets, in *Large Meteorite Impacts and Planetary Evolution*, Special Paper 293, Dressler, B. O., Grieve, R. A. F. and Sharpton, V. L., Eds., Geological Society of America, Boulder, CO, 1994, 29–50.
2. Baldwin, R. B., *The Face of the Moon*, Chicago, University of Chicago Press, 1949.
3. Breed, C. S. and Grow, T., Morphology and distribution of dunes in sand seas observed by remote sensing, in *A Study of Global Sand Seas*, McKee, E. D., Ed., U.S. Geological Survey, Professional Paper 1052, 1979.
4. Brodley, C. E., Lane, T., and Stough, T. M., Knowledge discovery and data mining, *Am. Sci.*, 87, 54–61, 1999.
5. Dence, M. R., A comparative structural and petrographic study of probable Canadian meteorite craters, *Meteoritics*, 2, 249–270, 1964.
6. Enzmann, R. D., Introduction to the section on signatures, *Ann. N. Y. Acad. Sci.*, 140(2), 154–156, 1966.
7. Evans, I. S., General geomorphometry, derivatives of altitude and descriptive statistics, in *Spatial Analysis in Geomorphology*, Chorley, R. J., Ed., Harper and Row, New York, 1972, 17–90.
8. Evans, I. S. and Cox, N. J., Geomorphometry and the operational definition of cirques. *Area*, 6, 150–153, 1974.
9. Fielder, G., The measurement of lunar altitudes by photography–I. Estimating the true lengths of shadows, *Planetary Space Sci.*, 9, 917–928, 1962.
10. Garvin, J. B. and Frawley, J. J., Geometric properties of Martian impact craters—preliminary results from the Mars Orbiter Laser Altimeter, *Geophysical Res. Lett.*, 25, 4405–4408, 1998.
11. Gelautz, M., Frick, H., Raggam, J., Burgstaller, J., and Leberl, F., SAR image simulation and analysis of alpine terrain, *ISPRS J. Photogrammetry Remote Sensing*, 53, 17–38, 1998.
12. Gibson, J. J., *The Perception of the Visual World*, Houghton–Mifflin, Boston, 1950.
13. Gilbert, G. K., The Moon's face, *Bull. Philos. Soc. Wash.*, 12, 241–292, 1893.
14. Green, J., Tidal and gravity effects intensifying lunar defluidization and volcanism, *Ann. N. Y. Acad. Sci.*, 123(2), 403–469, 1965.
15. Grieve, R., Terrestrial impact: the record in the rocks, *Meteoritics*, 26, 175–194, 1991.
16. Hartmann, W. K., Discovery of multi-ring basins: Gestalt perception in planetary science, in *Multi-Ring Basins, Proceedings Lunar and Planetary Science*, 12A, Schultz, P. H. and Merrill, R. B., Eds., Pergamon Press, New York, 1981, 79–90.
17. Hartmann, W. K. and Kuiper, G. P., Concentric structures surrounding lunar basins, *Commun. Lunar Planetary Lab.*, 1, 1962, 51–66.
18. Herrick, R. R. and Phillips, R. J., Implications of a global survey of Venusian impact craters, *Icarus*, 111, 387–416, 1994.
19. Hoffman, R. R., What's a hill? Computing the meaning of topographic and physiographic terms, in *Linguistic Approaches to Artificial Intelligence*, Schmitz, U., Schutz, R., and Kunz, A., Eds., Peter Lang Verlag, Frankfurt, 1990, 97–128.
20. Hoffman, R. R. and Pike, R. J., On the specification of the information available for the perception and description of the natural terrain, in *Local Applications of*

the Ecological Approach to Human-Machine Systems, Hancock, P., Flach, J., Caird, J., and Vicente, K., Eds., Erlbaum, Hillsdale, NJ, 1995, 285–323.
21. Horn, B. K. P. and Brooks, M. J., Eds., *Shape From Shading,* MIT Press, Cambridge, 1989.
22. Horton, R. E., Erosional development of streams and their drainage basins, hydrophysical approach to quantitative morphology, *Geol. Soc. Am. Bull.,* 56, 275–370, 1945.
23. Janes, D. M., Squyres, S. W., Bindschadler, D. L., Baer, G., Schubert, G., Sharpton, V. L., and Stofan, E. R., Geophysical models for the formation and evolution of coronae on Venus, *J. Geophysical Res.,* 97, 16,055–16,067, 1992.
24. Jarvis, R. S. and Clifford, N. J., Specific geomorphometry, in *Geomorphological Techniques,* Goudie, A. et al., Eds., Unwin Hyman, London, 1990, 63–70.
25. Johnson, G. G. and Vand, V., Application of a Fourier data smoothing technique to the meteoritic crater Ries Kessel, *J. Geophysical Res.,* 72, 1741–1750, 1967.
26. Knight, J., Morphological and morphometric analyses of drumlin bedforms in the Omagh Basin, north central Ireland, *Geografiska Annaler,* 79A, 255–266, 1997.
27. MacDonald, T. L., On the determination of relative lunar altitudes, *J. Br. Astronomical Assoc.,* 41, 367–379, 1931a.
28. MacDonald, T. L., The distribution of lunar altitudes, *J. Br. Astronomical Assoc.,* 41, 172–183 and 228–239, 1931b.
29. Melosh, H. J., *Impact Cratering—a Geologic Process,* Oxford University Press, New York, 1989.
30. Melosh, H. J., Missing rings, *Nature,* 368, 24, 1994.
31. Melosh, H. J., Multi-ringed revelation, *Nature,* 390, 439–440, 1997.
32. Melosh, H. J. and McKinnon, W. B., The mechanics of ringed basin formation, *Geophysical Res. Lett.,* 5, 985–988, 1978.
33. Melton, M. A., Correlation structure of morphometric properties of drainage systems and their controlling agents, *J. Geol.,* 66, 442–460, 1958.
34. Neuenschwander, G., Morphometrische Begriffe, eine kritische Übersicht auf Grund der Literatur, Universität Zürich, Inaugural-Dissertation, 1944.
35. Newman, E. B., Paradis, A. R., and Brabb, E. E., Feasibility and Cost of Using a Computer to Prepare Landslide Susceptibility Maps of the San Francisco Bay Region, California, U.S. Geological Survey, Bulletin 1443, 1978.
36. Nilsen, T. H., Wright, R. H., Vlasic, T. C., and Spangle, W. E., Relative Slope Stability and Land-Use Planning in the San Francisco Bay Region, California, U.S. Geological Survey, Professional Paper 944, 1979.
37. Nowicki, A. L., Lunar Topographic Mapping at the Army Map Service, U.S. Army Map Service, Washington, D.C., Technical Report 37, 1961.
38. Oreskes, N., *The Rejection of Continental Drift—Theory and Method in American Science,* Oxford University Press, New York, 1999.
39. Pike, R. J., Schroeter's rule and the modification of lunar crater impact morphology, *J. Geophysical Res.,* 72, 2099–2106, 1967.
40. Pike, R. J., Meteoritic Origin and Consequent Endogenic Modification of Large Lunar Craters—A Study in Analytical Geomorphology, U.S. Geological Survey, Open-file report 1158, 1969.
41. Pike, R. J., Geometric similitude of lunar and terrestrial craters, in *Proc. 24th Int. Geological Congr.,* 15, Montreal, Canada, 1972, 41–47.
42. Pike, R. J., Craters on Earth, Moon, and Mars—multivariate classification and mode of origin, *Earth Planetary Sci. Lett.,* 22, 245–255, 1974.

43. Pike, R. J., Volcanoes on the inner planets: some preliminary comparisons of gross topography, *Proc. 9th Lunar and Planetary Sci. Conf.*, Lunar and Planetary Institute, Houston, 1978, 3239–3273.
44. Pike, R. J., Apollo 15–17 Orbital Investigations—Geometric Interpretation of Lunar Craters, U.S. Geological Survey, Professional Paper 1046-C, 1980a.
45. Pike, R. J., Formation of complex impact craters: evidence from Mars and other planets, *Icarus*, 43, 1–19, 1980b.
46. Pike, R. J., Comment on "A schematic model of crater modification by gravity" by H. J. Melosh, *J. Geophysical Res.*, 88, 2500–2504, 1983.
47. Pike, R. J., Some morphologic systematics of complex impact structures, *Meteoritics*, 20, 49–68, 1985.
48. Pike, R. J., The geometric signature—quantifying landslide-terrain types from digital elevation models, *Mathematical Geol.*, 20, 491–511, 1988a.
49. Pike, R. J., Geomorphology of impact craters on Mercury, in *Mercury*, Vilas, F., Chapman, C. R., and Matthews, M. S., Eds., University of Arizona Press, Tucson, 1988b, 165–273.
50. Pike, R. J., Machine visualization of synoptic topography by digital image processing, Selected Papers in the Applied Computer Sciences 1992, Wiltshire, D. A., Ed., U.S. Geological Survey, Bulletin 2016, 1992, B1–B12.
51. Pike, R. J., Geomorphometry—progress, practice and prospect, in *Z. f. Geomorphologie N.F. Supple.-Bd.*, 101, Pike, R. J. and Dikau, R., Eds., 21–238, 1995.
52. Pike, R. J. and Spudis, P. D., Basin-ring spacing on the Moon, Mercury, and Mars, *Earth, Moon, Planets*, 39, 129–194, 1987.
53. Pohn, H. A. and Offield, T. W., Lunar Crater Morphology and Relative Age Determination of Lunar Geologic Units—Part 1, Classification, U.S. Geological Survey, Professional Paper, 700, C153–C162, 1970.
54. Pritt, M. D., Phase unwrapping by means of multigrid techniques for interferometric SAR, *IEEE Trans. Geoscience Remote Sensing*, 34, 728–738, 1996.
55. Rackham, T. W., Measurements and reductions of relative lunar altitudes, in *Measure of the Moon*, Kopal, Z. and Goudas, C., Eds., Gordon and Breach / Science Publishers, New York, 1967, 414–423.
56. Rodríguez-Iturbe, I., and Rinaldo, A., *Fractal River Basins: Chance and Self-Organization*, Cambridge University Press, Cambridge, 1997.
57. Sarnthein, M. and Walger, E., Der äolische Sandstrom aus der W-Sahara zur Atlantikküste, *Geologische Rundsch.*, 64, 1065–1087, 1975.
58. Schaber, G. G., Strom, R. G., Moore, H. J., Soderblom, L. A., Kirk, R. L., Chadwick, D. J., Dawson, D. D., Gaddis, L. R., Boyce, J. M., and Russell, J., Geology and distribution of impact craters on Venus—what are they telling us? *J. Geophysical Res.*, 97, 13,257–13,301, 1992.
59. Schenk, P. M., Crater formation and modification on the icy satellites of Uranus and Saturn—depth / diameter and central peak occurrence, *J. Geophysical Res.*, 94, 3813–3832, 1989.
60. Schröter, J. H. *Selenotopographische Fragmente zur genauern Kenntniss der Mondfläche, ihrer erlittenen Veränderungen und Atmosphäre, 1*, self-published, Helmstädt: Carl Gottfried Fleckeisen, Lilienthal, Germany, 1791.
61. Sharpton, V. L., Burke, K., Camargo-Zanoguera, A., Hall, S. A., Lee, D. S., Martin, L. E., Suarez-Reynoso, G., Quezada-Muneton, J. M., Spudis, P. D., and Urrutia-Fucugauchi, J., Chicxulub multi-ring impact basin: size and other characteristics derived from gravity analysis, *Science*, 261, 1564–1567, 1993.

62. Shoemaker, E. M., Interpretation of lunar craters, in *Physics and Astronomy of the Moon*, Kopal, Z., Ed., Academic Press, London, 1962, 283–359.
63. Spray, J. G. and Thompson, L. M., Friction melt distribution in a multi-ring impact basin, *Nature*, 373, 130–132, 1995.
64. Spudis, P. D., Comment concerning the review by W. B. McKinnon and R. Korotev of P. D. Spudis' book, *The Geology of Multi-Ring Basins*, *Geochimica Cosmochimica Acta*, 59, 2633–2635, 1995.
65. Watters, T. R. and Robinson, M. S., Radar and photoclinometric studies of wrinkle ridges on Mars, *J. Geophysical Res.*, 102, 10,889–10,903, 1997.
66. Welch, R., Jordan, T., Lang, H., and Murakami, H., ASTER as a source for topographic data in the late 1990s, *IEEE Trans. Geoscience Remote Sensing*, 36, 1282–1289, 1998.
67. Wilhelms, D. E., The Geologic History of the Moon, U.S. Geological Survey, Professional Paper 1348, 1987.
68. Williams, K. K. and Zuber, M. T., Measurement and analysis of lunar basin depths from Clementine altimetry, *Icarus*, 131, 107–122, 1998.
69. Zebker, H. A., Farr, T. G., Salazar, R. P., and Dixon, T. H., Mapping the world's topography using radar interferometry—the TOPSAT mission, *Proc. IEEE*, 82, 1774–1786, 1994.